System characterization of neuronal excitability in the hippocampus and its relevance to observed dynamics of spontaneous seizure-like transitions

2010 J. Neural Eng. 7 036002

(http://iopscience.iop.org/1741-2552/7/3/036002)

J. Neural Eng. **7** (2010) 036002 (15pp) doi:10.1088/1741-2560/7/3/036002

System characterization of neuronal excitability in the hippocampus and its relevance to observed dynamics of spontaneous seizure-like transitions

Osbert C Zalay[1], Demitre Serletis[1,2,3], Peter L Carlen[1,2,3] and Berj L Bardakjian[1,4]

[1] Institute of Biomaterials and Biomedical Engineering, University of Toronto, Toronto, M5S 3G9, Canada
[2] Toronto Western Research Institute, University Health Network, Toronto, M5T 2S8, Canada
[3] Department of Physiology, University of Toronto, Toronto, M5S 1A8, Canada
[4] Department of Electrical and Computer Engineering, University of Toronto, Toronto, M5S 3G4, Canada

E-mail: oz.zalay@utoronto.ca and berj@cbl.utoronto.ca

Received 4 December 2009
Accepted for publication 22 March 2010
Published 19 April 2010
Online at stacks.iop.org/JNE/7/036002

Abstract

Most forms of epilepsy are marked by seizure episodes that arise spontaneously. The low-magnesium/high-potassium (low-Mg^{2+}/high-K^{+}) experimental model of epilepsy is an acute model that produces spontaneous, recurring seizure-like events (SLEs). To elucidate the nature of spontaneous seizure transitions and their relationship to neuronal excitability, whole-cell recordings from the intact hippocampus were undertaken *in vitro*, and the response of hippocampal CA3 neurons to Gaussian white noise injection was obtained before and after treatment with various concentrations of low-Mg^{2+}/high-K^{+} solution. A second-order Volterra kernel model was estimated for each of the input–output response pairs. The spectral energy of the responses was also computed, providing a quantitative measure of neuronal excitability. Changes in duration and amplitude of the first-order kernel correlated positively with the spectral energy increase following treatment with low-Mg^{2+}/high-K^{+} solution, suggesting that variations in neuronal excitability are coded by the system kernels, in part by differences to the profile of the first-order kernel. In particular, kernel duration was more sensitive than amplitude to changes in spectral energy, and correlated more strongly with kernel area. An oscillator network model of the hippocampal CA3 was constructed to investigate the relationship of kernel duration to network excitability, and the model was able to generate spontaneous, recurrent SLEs by increasing the duration of a mode function analogous to the first-order kernel. Results from the model indicated that disruption to the dynamic balance of feedback was responsible for seizure-like transitions and the observed intermittency of SLEs. A physiological candidate for feedback imbalance consistent with the network model is the destabilizing interaction of extracellular potassium and paroxysmal neuronal activation. Altogether, these results (1) validate a mathematical model for epileptiform activity in the hippocampus by quantifying and subsequently correlating its behavior with an experimental, *in vitro* model of epilepsy; (2) elucidate a possible mechanism for epileptogenesis; and (3) pave the way for control studies in epilepsy utilizing the herein proposed experimental and mathematical setup.

1. Introduction

Epilepsy is a neurological disorder in which normal neuronal functions are interrupted by abnormal activity consisting of rhythmic, coordinated neuronal discharges. The characteristics of epilepsy vary widely, and while the disorder in many instances is linked to genetic factors, it can also be the result of a brain injury, environmental sensitizers, co-morbidity with another nervous system disease, or a combination thereof (Ottman *et al* 1996, Scharfman 2007). The symptoms, localization and spread of epileptic activity within the brain (e.g. generalized versus partial seizures) likewise differ from one form of epilepsy to another (Palmini *et al* 1991).

Despite the many manifestations of the disorder, experimental and computational models of epilepsy have indicated that epileptogenesis is in large part due to pathological disruption of the dynamic balance of excitation and inhibition that exists within or between neuronal ensembles in the brain (Chakravarthy *et al* 2009, Dudek and Staley 2007). For example, $GABA_A$ receptor antagonists, such as bicuculline (BC) or gabazine, disrupt inhibitory network functions and increase excitability, leading to the occurrence of seizure-like events (SLEs) (Behrens *et al* 2007). Similarly, extracellular low magnesium and elevated potassium *in vitro* epileptogenic preparations promote hyperexcitable conditions that favor the acute onset of spontaneous, recurrent SLEs (Derchansky *et al* 2004). Aberrant growth of recurrent excitatory synapses in certain regions of the brain, such as mossy-fiber sprouting in temporal lobe epilepsy (Sutula *et al* 1989), have also been implicated in epileptogenesis.

Therefore, as experimental and clinical evidence both suggest, the occurrence of epileptiform activity is coupled to a shift in network excitability that may have different root causes, but the observed dynamical effects are similar. If interconnected neuronal ensembles in the brain are treated as coupled network oscillators (Goutagny *et al* 2009, Buzsaki and Draguhn 2004, Derchansky *et al* 2006), then altering network properties in a coupled oscillator-type model to mimic changes in excitability under epileptogenic conditions should allow for reproduction of epileptiform phenomena.

In this article, we first examine neuronal excitability from a system-level standpoint using an *in vitro* intact hippocampal preparation of the low-Mg^{2+}/high-K^+ experimental model of epilepsy. We apply techniques of nonlinear system identification to derive a second-order Volterra kernel model from the response of CA3 *stratum pyramidale* neurons to Gaussian white noise (GWN) stimulation, and we compute the spectral energy of the response to assess differences in excitability before and after perfusion with low-Mg^{2+}/high-K^+ solution. In the low-Mg^{2+}/high-K^+ model of epilepsy, elevated extracellular potassium depolarizes neuronal membranes, which primes the biological network for activation, and a low extracellular magnesium concentration reduces Mg^{2+} blockade of post-synaptic N-methyl-D-aspartate (NMDA) receptor channels and magnesium-sensitive Ca^{2+} channels, increasing network susceptibility to depolarizing influences, as well as decreasing membrane charge-screening effects (Derchansky *et al* 2004). The combination produces hyperexcitable conditions in the network that can then be characterized by system identification.

We demonstrate that increased spectral energy of the neuronal response to GWN injection following low-Mg^{2+}/high-K^+ perfusion corresponds to increases in both the amplitude and the duration of the first-order Volterra kernel, but that kernel duration displays more sensitivity to changes in spectral energy (and hence excitability), and correlates better with overall changes in kernel size, as quantified by computing kernel area. By incorporating this relationship into the design and parameterization of an oscillator-type network model of the hippocampal CA3, we generate seizure-like activities in the computational model which resemble those of the experimental low-Mg^{2+}/high-K^+ model of epilepsy. Furthermore, we make use of the network to investigate the dynamics of spontaneous, recurrent seizure-like transitions and the factors that influence them—in particular, factors related to feedback regulation of network dynamics. Finally, we discuss a possible physiological basis for abnormal feedback regulation leading to seizure intermittency, involving the phasic interplay of extracellular potassium and neuronal activation.

2. Materials and methods

2.1. Whole-hippocampus preparation

Whole-intact hippocampi were prepared using a protocol adapted from a previous study (Derchansky *et al* 2004, Khalilov *et al* 1997). In accordance with the University Health Network Animal Care Committee's guidelines, C57/BL mice (P10−14) were anesthetized with halothane and decapitated, promptly followed by extraction of the brain from the cranial vault. The cerebellum was removed and the two cerebral hemispheres disconnected via sagittal transection. Each hemisphere was immersed for 5 min in ice-cold (2–5 °C), oxygenated (95% O_2/5% CO_2) artificial cerebrospinal fluid (ACSF) containing (in mM): 123 NaCl, 2.5 KCl, 1.5 $CaCl_2$, 2 $MgSO_4$, 25 $NaHCO_3$, 1.2 NaH_2PO_4 and 25 glucose (pH 7.4) (all chemicals were purchased from Sigma-Aldrich Canada Ltd). For each hemisphere, the hippocampus was exposed by medially displacing the midline structures using fine spatulas, under constant perfusion with ice-cold, oxygenated ACSF. Intact-hippocampal dissection was achieved by placing a cut in the septal region and ventrally extending this transection. Following disconnection, the whole hippocampus was isolated and immersed in room-temperature, oxygenated ACSF for at least 1 h prior to the start of any experimental recordings.

2.2. White noise experiments

Following incubation, the whole hippocampus was transferred to an RC-26 open bath recording chamber (Warner Instruments). Temperature in the chamber was maintained at 32.5 ± 0.5 °C via perfusion of warmed, oxygenated (95% O_2/5% CO_2) ACSF. The solution surface in the chamber was also oxygenated (95% O_2/5% CO_2) to minimize oxygen evaporation. Whole-cell patch-clamp recordings were performed on pyramidal cells within the *stratum pyramidale* of

the hippocampal CA3. Extracellular field potential recordings were collected by placing an extracellular electrode within the CA3 hippocampal region to confirm the occurrence of epileptiform activity at the local network level. An Olympus BX51WI upright microscope (Olympus Optical Co.) at 40× magnification (using a water-immersion lens) with an OLY-150IR camera-video monitor unit (Olympus Optical Co.) provided infra-red microscopy capability with differential interference contrast (IR-DIC) to visualize cells and electrode placement. A Digidata 1322A digitizer (for analog-to-digital conversion) and two Axopatch 200B amplifiers (Axon Instruments) were used to collect the whole-cell and extracellular field recordings under current clamp. Data was collected at a sampling rate of 10 kHz and subjected to a low-pass, 8-pole Bessel filter of 5 kHz with visualization in Clampfit 9.2 (Axon Instruments). 5–8 MΩ resistance electrodes were pulled from borosilicate capillary tubing (World Precision Instruments) using a Narishige PP-830 vertical puller. Intracellular solution in the recording pipette contained (in mM): 135 K-Gluconate, 10 NaCl, 1 $MgCl_2$, 2 Na_2ATP, 0.3 NaGTP (Tris), 10 NaHEPES, 0.5 EGTA and 0.0001 $CaCl_2$ (pH 7.4). Prior to patching each cell, seal resistance was confirmed to be 2–4 GΩ before breaking through the cellular membrane. Once patched, current pulses (±100 pA, 900 ms in duration at 50 pA increments) were used to determine the current–voltage relation and confirm cell identity. The computed average input resistance of the CA3 pyramidal neurons was 285.56 ± 28.63 MΩ (mean ± std. error; $N = 25$).

After 5 min of stable recording, repeat current pulses were administered to test cellular viability, followed by injection of action-potential (AP) subthreshold, bandlimited Gaussian white noise (GWN) impulse (1 nA peak-to-peak amplitude, 2 s duration) generated offline prior to the experiments using MATLAB 7.7 software (The MathWorks, Natick, MA). The perfusion solution was then switched to one of five increasingly epileptogenic solutions comprising an escalating gradient of low-Mg^{2+}/high-K^+ ACSF containing (in mM): (1) 1.5 $MgSO_4$/3 KCl; (2) 1.25 $MgSO_4$/3.5 KCl; (3) 1 $MgSO_4$/4 KCl; (4) 0.75 $MgSO_4$/4.5 KCl; and (5) 0.25 $MgSO_4$/5 KCl. Specimens were maintained under these conditions until an initial ictal-like episode or a period of increased excitability (enhanced spiking, bursting, etc.) was observed. Following termination of the episode or period, the specimen was left to stand for 1–2 min until quiescent interictal activity had resumed. During the interictal period, current-pulse injections were administered at regular intervals, followed by GWN stimulation (using the same 1 nA, 2 s stimulus impulse) while simultaneously recording the response. After sufficient recording time to capture excitable activity (e.g. ictal events, interictal spikes) and responses to GWN injection, ACSF washout was then applied to remove the epileptogenic solution.

2.3. Volterra kernel estimation

A second-order Volterra kernel model was estimated for each 2 s GWN input–output response pair (figure 1), using the Laguerre expansion technique (LET) (Marmarelis 1993). To summarize the technique, the sampled response of a causal nonlinear system to stimulus $x(t)$, under assumption of stationarity, is approximated by a discrete-time Volterra series of order N:

$$y(t) = q_o + \sum_{n=1}^{N} \sum_{\tau_1} \cdots \sum_{\tau_n} q_n(\tau_1, \ldots, \tau_n) \prod_{k=1}^{n} x(t-\tau_k) \quad (1)$$

where the nth-order kernels are expanded over a basis of discrete Laguerre functions, $L_j(\cdot)$, with coefficients $c_n(\cdot)$,

$$q_n(\tau_1, \ldots, \tau_n) = \sum_{j_1} \cdots \sum_{j_n} c_n(j_1, \ldots, j_n) \prod_{k=1}^{n} L_{j_k}(\tau_k). \quad (2)$$

The N_L discrete Laguerre functions used in the expansion ($j = 0, 1, 2, \ldots, N_L - 1$) are derived from the following expression (Ogura 1985):

$$L_j(\tau) = \sqrt{\alpha^{\tau-j}(1-\alpha)} \cdot \sum_{m=0}^{j} (-1)^m \times \binom{\tau}{m} \binom{j}{m} \alpha^{j-m} (1-\alpha)^m \quad (3)$$

where $0 < \alpha < 1$ is the parameter controlling the decay rate of the basis functions. To obtain estimates of the kernels, the expansion coefficients $c_n(\cdot)$ and q_o are fitted by least-squares regression of the input–output response pair using Gaussian white noise as the input stimulus. Recorded traces from the whole hippocampus were first high-pass filtered at a 4 Hz cut-off using a very high order digital finite impulse response filter, to remove the non-stimulus-related 0–4 Hz rhythm intrinsic to the intact hippocampus (Wu *et al* 2002). The presence of the low-frequency intrinsic rhythm would have otherwise affected the accuracy of the kernel estimates. Each recorded response was divided into two equal segments of 10 000 samples (1 s duration) to serve as estimation (kernel-model fitting) and testing (prediction) segments, respectively. The parameters for LET, N_L and α, were chosen in an unsupervised manner using a non-gradient pattern search (Hooke and Jeeves 1961) which minimized the prediction error from the kernel model in the testing segment. Initial guess values of $N_L = 10$ and $\alpha = 0.5$ were used to seed the optimization runs. In general, the second-order LET model yielded the lowest estimation and prediction errors, when both the first and second-order kernels were used to fit and generate the output—as opposed to using only the first-order kernel from the second-order fitted model, or applying standard deconvolution to get the linear impulse response (figure 1(D)). Nevertheless, the linear component comprised the largest portion of the response generated under AP subthreshold conditions.

2.4. Kernel dimensions and spectral energy

Once an optimal kernel model was determined, the dimensions of the first-order kernel were computed, namely (1) the peak kernel amplitude; and (2) the time duration of the kernel, as measured from $t = 0$ to $t = \tau$, where τ is the time taken for the kernel to decay to $1/e$ of its peak value. The pre- and post-treatment kernel pairs (i.e. before and after perfusion with low-Mg^{2+}/high-K^+ solution, replacing

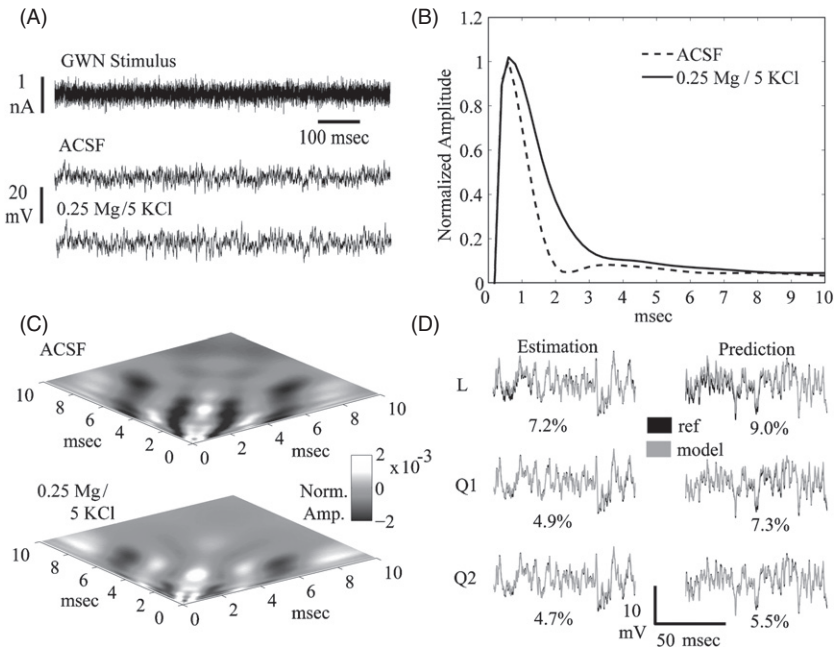

Figure 1. White noise experiment with estimation of second-order kernel model using the Laguerre expansion technique (LET). (A) Bandlimited Gaussian white noise stimulus (top trace) and corresponding responses of a *stratum pyramidale* neuron under standard ACSF perfusion (middle), and under 0.25 mM $MgSO_4$/5 mM KCl perfusion (bottom) during an interictal epoch. (B) Estimated first-order Volterra kernels pre- and post-treatment with epileptogenic solution. (C) Estimated second-order Volterra kernels pre- and post-treatment. (D) Comparison of fitting and prediction error for 0.25 mM $MgSO_4$/5 mM KCl using linear deconvolution (L), the first-order LET kernel only (Q1), and the full second-order LET model (Q2). Amplitudes of the kernels in (B) and (C) are normalized to the peak of the first-order ACSF kernel.

standard ACSF solution) were normalized in amplitude and time by dividing by the largest peak amplitude and longest kernel duration of the pre-treatment (ACSF) controls, respectively, covering all samples across the five low-Mg^{2+}/high-K^+ perfusion concentration groupings ($N = 25$). The resultant normalized kernel amplitude and duration values were dimensionless. This normalization procedure ensured the relative differences between the pre- and post-treatment kernels were preserved for comparison purposes, and also permitted comparisons to be made between the different concentration groupings. To obtain a measure of neuronal excitability from the recorded responses to GWN, the spectral energy of the pre- and post-treatment responses was calculated using Parseval's theorem. This allowed for the spectral energy to be directly estimated from the area under the curve of the squared magnitude of the response. A measured change in spectral energy of the post-treatment response would indicate a difference in excitability due to increased/decreased amplitude and/or frequency content of the response to the same GWN input, which could then be correlated with changes in either kernel amplitude or duration.

2.5. Network model of the hippocampus

The area CA3 of the hippocampus presents as an auto-associative network (Hasselmo *et al* 1995). There are recurrent excitatory synapses between pyramidal neurons, and the network is subject to GABAergic inhibitory feedback from interneurons. The CA3 is also rhythmically active, able to generate and sustain intrinsic population oscillations (Kubota *et al* 2003, Buzsaki 2002, Strata 1998). To model the circuitry and rhythmicity of the CA3 at a systems level, an oscillator-type model comprising four interconnected units was constructed (figure 4). Two of the network units have auto-associative self-feedback and mutual reciprocal connectivity, while the remaining two units oppose the activity of the first two units through negative feedback emulating GABAergic feedback from interneurons.

The specific design of the units is adapted from the cognitive rhythm generator (CRG) (Zalay and Bardakjian 2009), itself a development of the mapped clock oscillator (Bardakjian and Diamant 1994, Zalay and Bardakjian 2008), featuring second-order limit cycle dynamics and an output static nonlinearity (see (11) below) mapping the internal state variables to an observable output waveform. Coupling between CRGs in the network model occurs through an exponential impulse response function, referred to here as an 'integrating mode', which has equivalent functionality to the first-order kernel. The operation of convolution between the mode and its inputs is dynamically represented by second-order dynamics. Therefore, the system of four differential equations defining the combined dynamics of the nth CRG is as follows:

$$\dot{u}_{1n} = \omega_n\left\{u_{2n}(1 + S_{\phi,n}) + u_{1n}\left(1 + S_{\alpha,n} - u_{1n}^2 - u_{2n}^2\right)\right\} \quad (4)$$

$$\dot{u}_{2n} = \omega_n\left\{-u_{1n}(1 + S_{\phi,n}) + u_{2n}\left(1 + S_{\alpha,n} - u_{1n}^2 - u_{2n}^2\right)\right\} \quad (5)$$

$$\dot{u}_{3n} = u_{4n} \quad (6)$$

$$\dot{u}_{4n} = \beta_n F_n - 2\beta_n u_{4n} - \beta_n^2 u_{3n} \quad (7)$$

Table 1. CRG hippocampal network model parameters.

Parameter name	Symbol(s)	Value
Intrinsic oscillator frequency	ω_1, ω_2	2π
	ω_3, ω_4	2.2π
Constant offset	c_{01}, c_{02}	-0.2
	c_{03}, c_{04}	0
Coupling constant	$c_{11}, c_{12}, c_{21}, c_{22}$	0.5
	$c_{13}, c_{14}, c_{23}, c_{24}$	0.3
	$c_{31}, c_{32}, c_{41}, c_{42}$	-0.75
Modulatory gain	k_1, k_2, k_3, k_4	15
Mode decay constant	$\beta_1,\beta_2,\beta_3,\beta_4$	β[a]

[a] The value of β depends on conditions being modeled.

where ω_n is the intrinsic angular oscillator frequency, and $S_{\phi,n}$ and $S_{\alpha,n}$ are the phase and amplitude modulation functions, respectively, defined in this paper as

$$S_{\phi,n} = c_{0n} + k_n u_{3n} + \tilde{x}_n(t) \tag{8}$$

$$S_{\alpha,n} = 0 \tag{9}$$

with modulatory gain, k_n, and optional additive input, $\tilde{x}_n(t)$. β_n is the parameter controlling the decay rate of the mode response. For the specific hippocampal network model, all mode decay constants are set to the same value, β, which is dependent on the conditions being modeled. Table 1 lists the model parameters and their respective values. The state variables u_{1n} and u_{2n} belong to the limit cycle stage and together define the instantaneous position of the rotor in terms of its amplitude and phase; u_{3n} and u_{4n} are the mode response variables, with u_{3n} representing the instantaneous response amplitude, and u_{4n}, its rate of change. F_n is the mode input function written as a linear combination of CRG outputs (y_m), directional coupling coefficients (c_{mn}), and an optional external input, $x_n(t)$,

$$F_n = \sum_{m=1}^{M} c_{mn} y_m + x_n(t). \tag{10}$$

The static nonlinearity (mapper) that defines the output of the nth CRG is as follows:

$$y_n = c_{0n} + u_{3n} + \sqrt{u_{1n}^2 + u_{2n}^2}\, W\left(\arctan\frac{u_{2n}}{u_{1n}}\right) \tag{11}$$

where c_{0n} is a constant offset, $W(\cdot)$ is the intrinsic output waveform of the CRG normalized over $(-\pi, \pi]$ (Zalay and Bardakjian 2009), with the 4-quadrant arctangent function providing the instantaneous phase angle.

2.6. Complexity analysis of model-generated signals and in vitro experimental data

A maximum Lyapunov exponent measure was applied to classify dynamics at spontaneous seizure-like transitions. The maximum Lyapunov exponent, λ, quantifies the exponential rate of separation of nearby trajectories in state space. The hallmark of complex, possibly chaotic dynamics is a positive maximum Lyapunov exponent coinciding with trajectories that remain bounded. If $\|\delta\mathbf{X}(0)\|$ is the initial magnitude of the separation vector between two points on neighboring trajectories at time 0, then at time t the separation magnitude is given by

$$\|\delta\mathbf{X}(t)\| = \|\delta\mathbf{X}(0)\|\, b^{\lambda t} \tag{12}$$

where b is a positive real-valued number. In theory, computing the maximum Lyapunov exponent from (12) requires a stationary, noise-free process in the limit of infinite time and infinitesimal separation. For practical signals, an averaged estimate of the maximum Lyapunov exponent over many finite time segments may be defined:

$$\lambda = \frac{1}{N\Delta t}\sum_{i=1}^{N} \log_b \frac{\|\delta\mathbf{X}_i(\Delta t)\|}{\|\delta\mathbf{X}_i(0)\|} \tag{13}$$

whereby the test point, $\mathbf{X}_j$, on a neighboring trajectory relative to the ith reference point, $\mathbf{X}_i$, is selected such that $\|\delta\mathbf{X}_i(0)\| = \min\|\mathbf{X}_i - \mathbf{X}_j\|$, $j \neq i$ and $\langle\delta\mathbf{X}_i(0), \delta\mathbf{X}_{i-1}(\Delta t)\rangle/(\|\delta\mathbf{X}_i(0)\| \cdot \|\delta\mathbf{X}_{i-1}(\Delta t)\|) \sim 1$ (the angled brackets denote the inner product). Additionally, a lower bound on the magnitude of $\delta\mathbf{X}_i(0)$ may be specified to compensate for the effect of noise on the estimate. For this study, the method of computing λ was adapted from the *STLmax* algorithm for determining the maximum Lyapunov exponent of a short time series (Iasemidis *et al* 2000). A sliding-window version of the measure was implemented for capturing dynamic transitions. The method of time-delay embedding was used to construct the phase-space representations of the time series for analysis.

A second measure related to the fractal structure of a signal was also applied to compare biological and model-generated time series. The pointwise Hölder exponent, which is a measure of the regularity of a signal around each point, was computed using the FRACLAB software toolbox developed by Legrand *et al* at Team Complex, INRIA. The pointwise Hölder exponent, h, of signal $y(t)$ at time t is defined as the supremum exponent value for which $y(t)$ is Lipshitz; that is, there exists some positive constant, c, such that for a given neighborhood $\hat{t}$ of t,

$$|y(t) - y(\hat{t})| \leqslant c|t - \hat{t}|^h \tag{14}$$

for all $\hat{t}$. The smaller the Hölder exponent, the rougher and more irregular the signal about time t. Practically, a reliable method for estimating $h \in [0,1]$ is to analyze the local oscillations in the signal about each time point (Trujillo *et al* 2007). Specifically, the Hölder condition (14) can be rephrased such that h is determined by satisfying

$$g_\varepsilon(t) \leqslant c\varepsilon^h \tag{15}$$

where

$$g_\varepsilon(t) = \sup\{|y(t_a) - y(t_b)|\}, \qquad t_a, t_b \in [t - \varepsilon, t + \varepsilon]. \tag{16}$$

The function $g_\varepsilon(t)$ relates to the magnitude of the fluctuation in the neighborhood defined by ε, and so h is established by sampling neighborhoods of different radius about t, and computing the slope of the linear regression of $\log(g_\varepsilon(t))$ versus $\log(\varepsilon)$ in accordance with (15).

3. Results

3.1. System characterization of neuronal excitability

The Gaussian white noise (GWN) experiments were performed on five groups of *stratum pyrimidale* neurons

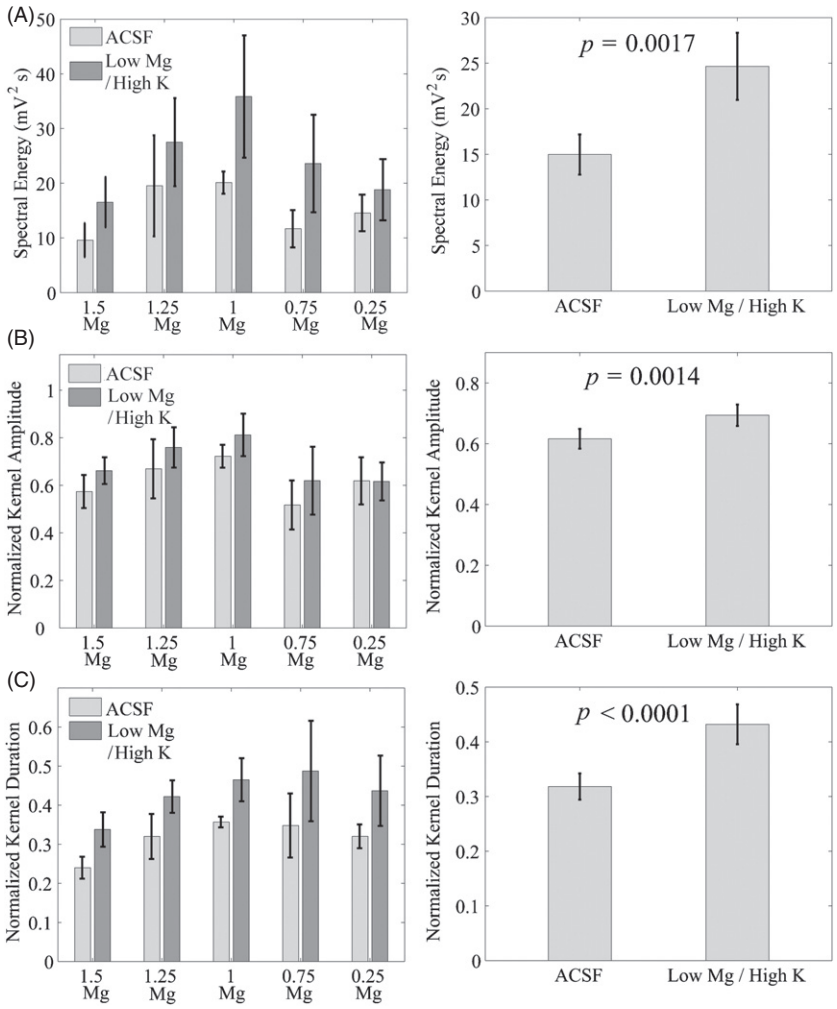

Figure 2. Pre- and post-epileptogenic treatment spectral energy and first-order kernel dimensions for the five low-Mg^{2+}/high-K^+ concentration groupings (see section 2): 1.5 Mg, 1.25 Mg and 1 Mg ($N = 5$ each); 0.75 Mg ($N = 6$); and 0.25 Mg ($N = 4$). (A) Estimated spectral energies of the response to GWN; overall change is significant ($p = 0.0017$, two-sided paired t-test pre- and post-treatment for all samples, $N = 25$). (B) First-order kernel peak amplitudes, normalized to largest ACSF kernel amplitude over all treatment samples. (C) First-order kernel durations, normalized to longest ACSF kernel duration over all treatment samples. Error bars are standard error of the mean.

pertaining to the five epileptogenic low-Mg^{2+}/high-K^+ perfusion concentrations (see section 2). The 1.5, 1.25 and 1 mM $MgSO_4$ perfusion groups each had a sample size of five neurons, six neurons were tested in the 0.75 mM group and four were tested in the 0.25 mM group, for a total of $N = 25$ samples. The response of the neurons to GWN recorded under standard ACSF perfusion served as the control. Figure 1 shows example traces and kernels from a GWN experiment using the 0.25 mM $MgSO_4$ perfusion solution. Nonlinear system identification of each of the GWN input–output response pairs (before and after epileptogenic treatment) yielded a second-order kernel model, but only the first-order kernel was considered because the linear component accounts for the majority of the response under AP subthreshold stimulation (figures 1(B)–(D)).

Visually, the first-order kernels estimated under low-Mg^{2+}/high-K^+ conditions were typically broader and slightly larger in amplitude relative to kernels measured under standard ACSF perfusion (figure 2(B)) (see Kang *et al* 2010). These observations were validated by measuring increases in the peak amplitude and time duration of the post-treatment kernels (figures 2(B) and (C)), which were statistically significant ($p = 0.0014$ and $p < 0.0001$, respectively). Cell-to-cell variability, however, prevented recognition of a clear trend across the five perfusion concentration groupings, because of variation in the ACSF controls between groups. Estimation of the spectral energy content of the neuronal responses to GWN stimulation showed a similar increase for the post-treatment responses relative to the ACSF control responses, for all treatment groups (figure 2(A)) ($p = 0.0017$). Again, no dose-response could be discerned because of cell-to-cell variability.

By inspection, it is difficult to conclude whether a definitive relationship exists between the spectral energy of the neuronal response to GWN stimulation, a quantifier of neuronal excitability, and either of the two measured attributes of the first-order kernel. Also not known is which one of the attributes—kernel amplitude or kernel duration—plays the more predominant role in such a relationship. However, once values of the measurements were re-cast in terms of the percentage change with respect pre- and post-treatment cases and plotted against one another, a linear relationship

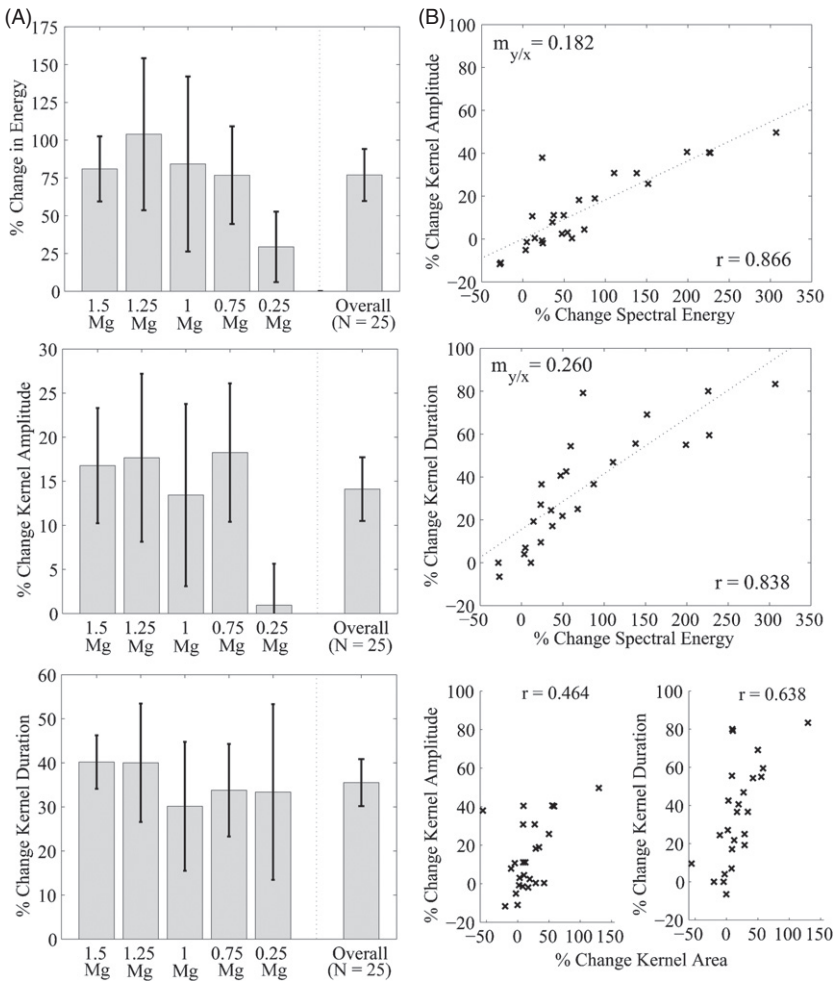

Figure 3. (A) Percent change in spectral energy and first-order kernel dimensions post-treatment (relative to ACSF control) for various concentrations of low-Mg^{2+}/high-K (see section 2). (B) Percent change in kernel dimensions versus percent change in spectral energy. Both kernel amplitude and duration are positively correlated (Pearson correlation coefficient: $r = 0.866$ and 0.838, respectively; $p < 0.0001$, one-sided *t*-test, alternative hypothesis of positive correlation) but relative change in duration is more pronounced, as determined from the respective slopes, $m_{y/x} = 0.182$ and 0.260, and correlates more directly with changes in kernel area: $r = 0.464$ ($p = 0.0097$) versus $r = 0.638$ ($p = 0.0003$).

emerged whereby increasing spectral energy correlated with both increasing kernel amplitude and duration (figure 3). This result was not entirely unexpected, as the larger response energy should be associated with increased kernel size. What is relevant, however, is that the relative change in duration of the first-order kernel was more sensitive than kernel amplitude to changes in spectral energy, as quantified by its larger slope ($m_{y/x} = 0.260$); furthermore, increased kernel duration was more strongly correlated with increased kernel area (Pearson correlation coefficient $r = 0.638$ for the duration versus $r = 0.464$ for the amplitude)—area being a measure of overall kernel size, computed numerically using the trapezoidal rule. Therefore, changes in size of the kernel appear to relate more closely to changes in kernel duration than to changes in kernel amplitude, and increased kernel size relates to increased spectral energy of the response, and hence increased excitability. This implies that the changes in kernel duration are a system manifestation of changes in neuronal excitability. This relationship was subsequently exploited in the development of the cognitive rhythm generator (CRG) network model of the hippocampal CA3, in which the effect of changing network excitability could be explored by varying the mode decay constant, β (figure 4), thereby controlling the decay length and area under the curve of the exponential integrating mode.

3.2. Evaluation of network model and biological neurodynamics

At a relatively high value of $\beta = 20$, and consequently relatively low network excitability, the network model activity is interictal-like, characterized by irregular, uncoordinated spiking. A simulated extracellular field potential (EC) was included to obtain an overview of the combined population dynamics. The EC trace was created by treating the CRGs as point sources spaced symmetrically apart, with the imaginary extracellular electrode placed at the center above the network. Each source output was differentiated twice and summed together to produce the pseudo extracellular field signal (Wilson and Bower 1992, Zalay and Bardakjian 2008). During interictal-like activity, the field consists of low-amplitude ripples and fluctuations that are random in appearance because

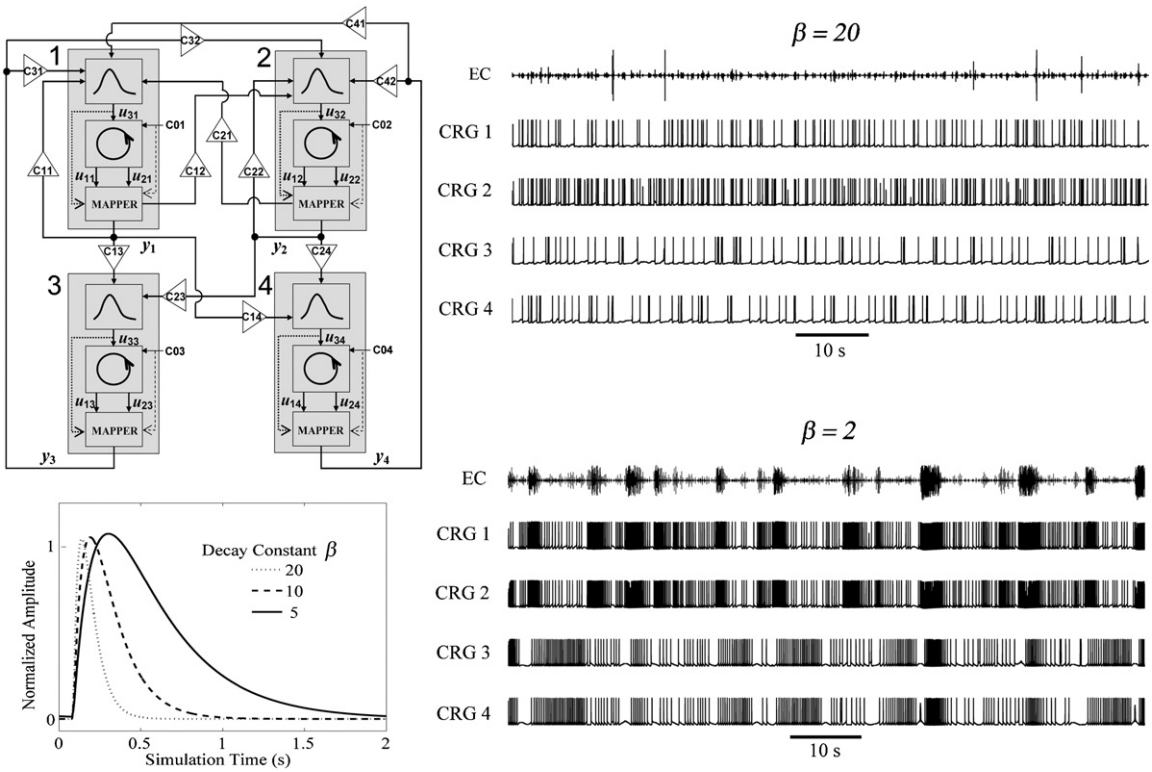

Figure 4. Cognitive rhythm-generator (CRG) model of a hippocampal network exhibiting interictal-like spiking ($\beta = 20$) and spontaneous, recurrent seizure-like events (SLEs) ($\beta = 2$); the outputs of each unit, consisting of an input mode, a limit-cycle rotor and an output-stage static nonlinearity (mapper), are shown alongside the simulated extracellular field potential (EC). The integrating mode decay is controlled by β.

the CRG outputs are complex, and entrainment between units is low. Decreasing the value to $\beta = 2$ increases the integrating mode decay length—analogous to an increase in duration and size of the first-order kernel in terms of effect—and this causes network activity to become epileptiform in character, with the sudden onset of spontaneous, intermittent seizure-like events (SLEs). The ictal-like discharges that occur synchronously in two or more network CRGs show up the in the pseudo extracellular field potential as dense, large-amplitude spike clusters, because of the effect of summation. Therefore, the field trace enables visualization of when network activity is most strongly entrained and rhythmic, corresponding to SLE occurrence.

The characteristics of the SLEs produced by the hippocampal CA3 network model are similar to those observed from the experimental low-Mg^{2+}/high-K^+ model of epilepsy, for which seizure onset occurs shortly after application of the epileptogenic solution, and seizures are also recurrent and spontaneous. Although not all CA3 neurons sampled during the white noise experiments expressed SLEs, SLEs were observed from all low-Mg^{2+}/high-K^+ treatment groups, irrespective of dosage. Figures 5(A)–(D) provide a qualitative comparison of experimental SLEs recorded from the hippocampus and SLEs produced by the CRG network model, depicting similarities in their waveforms and appearance. Complexity analysis was undertaken on the respective biological and model time series to enable quantitative comparison of dynamics on a sample-by-sample basis (figure 6). When time scales diverged significantly, the reference signal was re-sampled to maintain equivalency in comparison.

Figure 6(A) demonstrates the spontaneous transition from interictal to ictal dynamics in a hippocampal CA3 pyramid is marked by a clear decrease in the maximum Lyapunov exponent (bits/sample), as estimated from the phase signal, $\varphi(t)$, of the original time series, $y(t)$. This is consistent with experimental evidence of a drop in dynamic complexity associated with seizure epochs (Bergey and Franaszczuk 2001, Chiu *et al* 2006, Nair *et al* 2009). The phase signal was obtained using the Hilbert Transform,

$$\varphi(t) = \arctan \frac{\hat{y}(t)}{y(t)} \tag{17}$$

$$\hat{y}(t) = \frac{1}{\pi} \lim_{\varepsilon \to 0^+} \left(\int_{t-1/\varepsilon}^{t-\varepsilon} \frac{y(\tau)}{t-\tau} \, \mathrm{d}\tau + \int_{t+\varepsilon}^{t+1/\varepsilon} \frac{y(\tau)}{t-\tau} \, \mathrm{d}\tau \right) \tag{18}$$

where (18) is a convolution between $y(t)$ and the Hilbert impulse function $1/(\pi t)$ that was implemented for discrete-time signals using a fast Fourier transform method for computing the transform (Marple 1999). Performing the maximum Lyapunov exponent estimation on the phase signal rather than the original time series places emphasis on phase variations rather than amplitude variations within the signal when quantifying dynamic transitions between higher complexity, interictal activity and lower complexity, more regular ictal episodes. Figure 6(B) reveals that the CRG network model was able to capture the decline in complexity coinciding with a spontaneous SLE onset, as determined

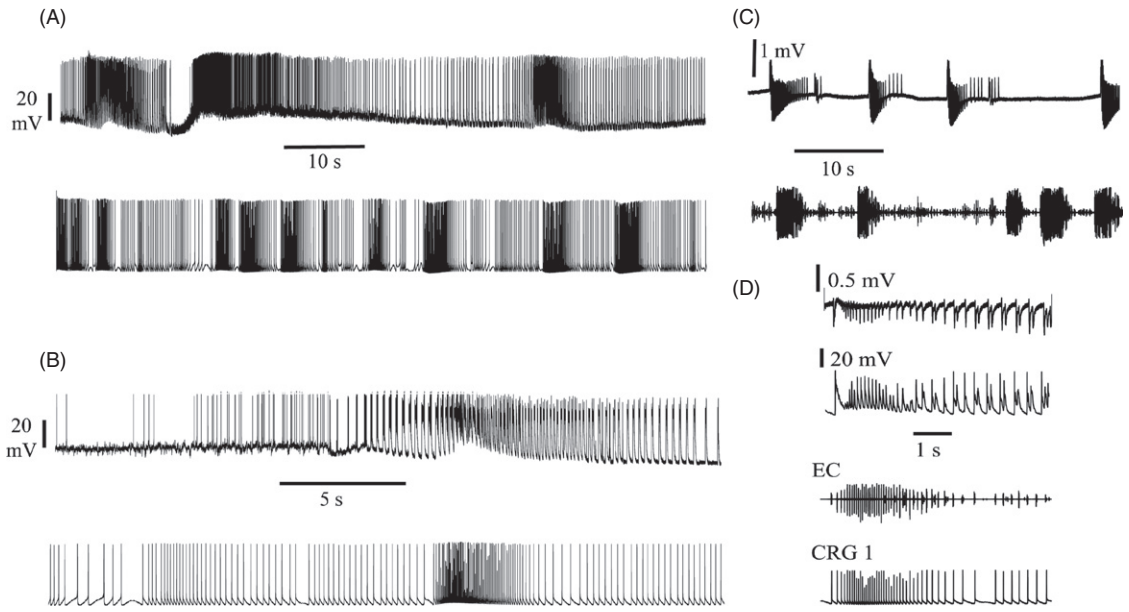

Figure 5. Comparison of experimental low-Mg^{2+}/high-K^{+} model to the cognitive-rhythm generator (CRG) hippocampal network model. (A) Intermittent seizure-like transitions in a whole-cell recording from the *stratum pyramidale* (top) and the CRG model (bottom). (B) Close-up view of a single seizure-like event (SLE) in the experimental trace (top) and the simulated version (bottom). (C) Extracellular recording from the *stratum pyramidale* showing recurrent SLEs (top) and pseudo extracellular field (EC) of recurrent SLEs in CRG model (bottom). The experimental trace has been de-trended to remove large-scale baseline deflections for comparison purposes. (D) Correspondence of local field potential and intracellular trace from experiment (top pair) and CRG model (bottom pair).

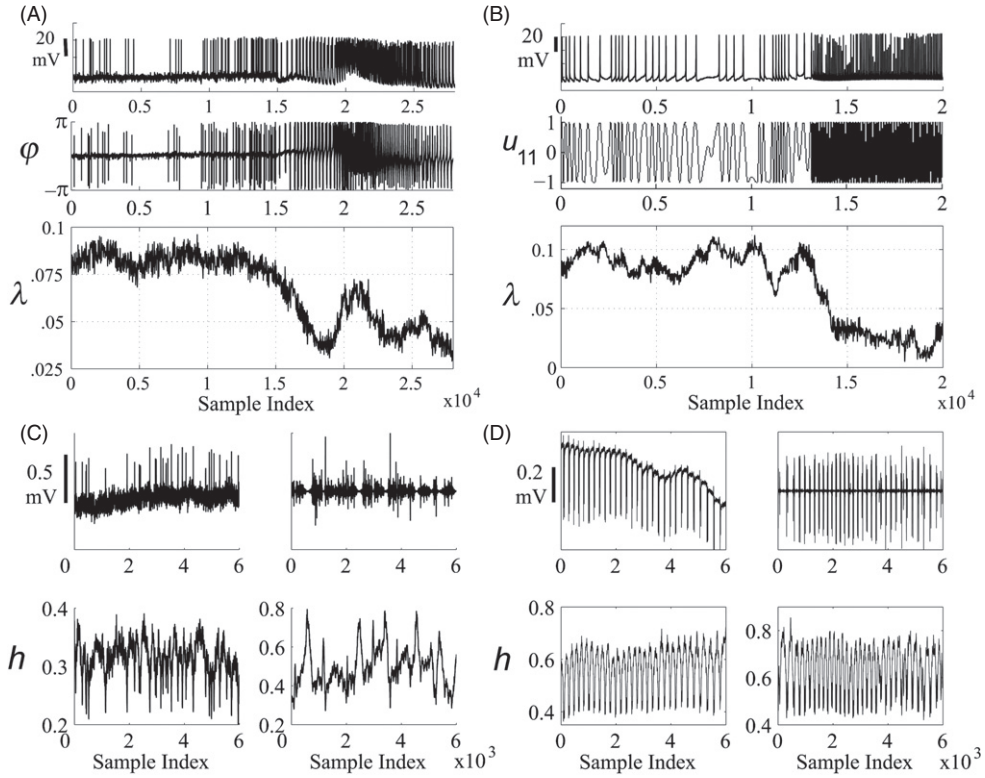

Figure 6. Quantitative comparison of biological and model dynamics. (A) Maximum Lyapunov exponent analysis of the dynamic transition to seizure in a CA3 pyramidal neuron, performed on the Hilbert transform-derived phase signal, φ. The exponent, λ, shows a characteristic decrease at ictal onset. (B) Maximum Lyapunov exponent analysis of an SLE transition in the hippocampal network model, performed on state variable u_{11}. (C) Pointwise Hölder exponent, h, of extracellular field potential during interictal spiking for biological recording (left column) and model trace (right column). (D) Pointwise Hölder exponent analysis of an ictal epoch, presented as in (C).

Table 2. Pointwise Hölder exponent measures ($N = 6000$ per series).

Data	Mean	St. dev.	Skew	Kurtosis	Max	Min	Range
GWN	0.17	0.016	0.035	2.89	0.23	0.12	0.11
MBM	0.52	0.089	0.78	2.22	0.75	0.38	0.42
Ref. Interictal	0.31	0.030	−0.66	3.55	0.39	0.20	0.19
Model Interictal	0.49	0.10	0.55	2.99	0.79	0.27	0.52
Ref. Ictal	0.57	0.083	−0.68	2.33	0.73	0.36	0.37
Model Ictal	0.64	0.099	−0.42	1.99	0.85	0.42	0.43

from maximum Lyapunov exponent analysis of the u_{11} state variable.

Correspondence of the dynamic features of the interictal and ictal epochs was also observed to an extent in the network model, as shown from the pointwise Hölder exponent values of the extracellular field potential recorded experimentally and simulated in the model (figures 6(C) and (D)). The results of the comparison are provided in table 2, along with values from a monofractal white noise process and a multifractal Brownian process for reference. For the ictal epoch, time-evolution of the Hölder exponents in both the biological and model cases is comparable, as are the mean and spread of the exponent values. For the interictal epoch, the model and experimental traces each display Hölder exponent values with a lower mean in comparison to their ictal counterpart, with the biological interictal time series assuming lower values and spread than the model interictal time series, exhibiting dynamics that are closer to the white noise reference. Part of the explanation why the model interictal has a larger spread and higher mean than the experimental interictal reference is that the model network activity exhibits quiescent periods; the experimental interictal activity on the other hand is more or less continuous. The quiescent periods are marked by high exponent values (∼0.8) which differ from the more active regions with lower exponent values (∼0.3–0.5), hence affecting the statistics. One reason for the punctuated interictal model activity is the small size of the model network. As the extracellular field potential relates to the summed activity over all network units, a small network of four units cannot generate the kind of continuous field-potential activity that a much larger network, such as the intact hippocampus, can generate.

3.3. Non-spontaneous dynamic transitions in the model

The transitions between interictal-like and ictal-like activity that occur spontaneously in the CRG network model do so within limited regions of the parameter space, requiring appropriate coupling values and a low to moderate range of β. Other combinations of coupling and/or model parameterization produce different network dynamics, including regular spiking or bursting, mixed interictal-like spiking and bursting, and dense interictal-like spiking (figure 7(A)). Parameter changes affecting model system behavior through alteration of network properties or connectivity are analogous to neurophysiological mechanisms of short-term and long-term plasticity (Carvalho and Buonomano 2009, Gaiarsa *et al* 2002, Varela *et al* 1997), as well as pharmacological manipulations targeting specific cell types or connections (Kim *et al* 1997, Marder and Thirumalai 2002). At higher values of β, the network activity is more irregular and interictal-like for reduced magnitudes of negative coupling from CRG 3 and CRG 4, and more rhythmic for larger magnitudes of negative coupling. The opposite is true at low values of β. Dynamic transitions into and out of SLEs at low β depend on the presence of opposing feedback. Without counter feedback, the network becomes locked into a regimen of tonic, regular spiking. At even smaller levels of β and negative coupling, the network becomes asymptotically unstable and breaks down. Therefore, the right blend of interactions between positive and negative, 'push-and-pull' forces within the network is needed to initiate and sustain recurrent SLEs.

Excitation by an external stimulus and perturbations with additive noise are other means by which non-spontaneous dynamic transitions can be effected in the model. Addition of discrete shot-noise (SN) to the phase-modulation function, $S_{\phi,n}$, of each CRG unit within the network can induce seizure-like transitions under simulated epileptogenic conditions (i.e. conditions produced by small values of β and moderate to strong coupling) (see figure 7(B)).

3.4. Mechanism of spontaneous seizure-like transitions

To understand the mechanism of spontaneous recurrent seizure-like transitions first requires investigation of the dynamic properties of the isolated CRG. The dynamics of the single, isolated CRG, without coupling support are represented by (4) and (5). The physiological analogue is a neuron or ensemble of neurons functioning as an independently rhythmic unit, isolated from the rest of the network, with spontaneous activity manifesting as intrinsic oscillations. Taking the Jacobian of the second-order system yields

$$J = \omega_n \begin{bmatrix} 1 + S_{\alpha,n} - 3u_{1n}^2 - u_{2n}^2 & 1 + S_{\phi,n} - 2u_{1n}u_{2n} \\ -1 - S_{\phi,n} - 2u_{1n}u_{2n} & 1 + S_{\alpha,n} - 3u_{2n}^2 - u_{1n}^2 \end{bmatrix} \tag{19}$$

and solving for the eigenvalues of (19) at (0,0) gives

$$\xi_{1,2} = \omega_n[(1 + S_{\alpha,n}) \pm (1 + S_{\phi,n})i]. \tag{20}$$

The eigenvalues reveal that (0,0) is an unstable focus under unperturbed conditions ($S_{\alpha,n} = S_{\phi,n} = 0$, $(1 + S_{\alpha,n}) > 0$ and $(1 + S_{\phi,n}) \neq 0$), at the center of a stable limit cycle of radius 1. A supercritical Hopf bifurcation occurs at $S_{\alpha,n} = -1$, whereby the limit cycle vanishes when $S_{\alpha,n} < -1$ and the origin becomes a stable focus. Varying $S_{\phi,n}$ does not

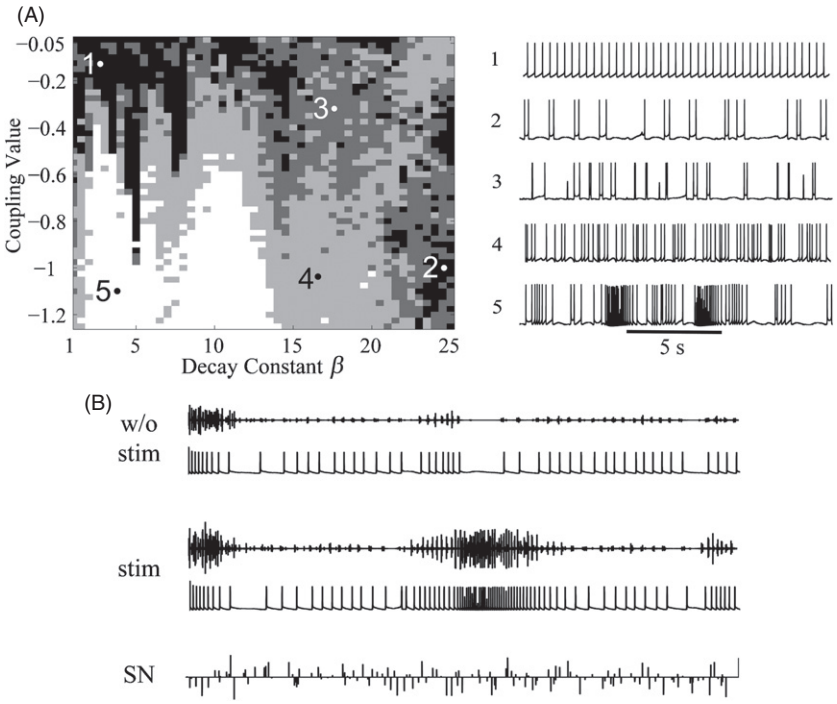

Figure 7. Non-spontaneous dynamic transitions in the hippocampal network model. (a) Parameter-dependent transitions involving different combinations of negative feedback coupling and mode decay constant, β, produce varying network dynamics; *black*: regular spiking or bursting; *dark gray*: mixed interictal; *light gray*: dense interictal; *white*: epileptiform activity. Sample traces corresponding to coordinates marked on the map are shown below. (B) A seizure-like event is induced by additive shot noise (SN) of variance 0.01, administered simultaneously to all four CRG units ($\beta = 2$). Using identical parameterization and initial conditions, no transition occurred for the case without stimulation, whereas the SN-stimulated network generated an SLE.

change the stability of the fixed point but the direction of phase rotation reverses as $S_{\phi,n}$ crosses -1, with the phase sticking at $S_{\phi,n} = -1$. For the coupled network case, the fixed point at the origin is replaced by one or more saddle equilibria, with their distribution depending on network parameterization and topology. For the hippocampal network model of figure 4, multiple saddle foci were found using Newton's method, each possessing a mixture of real and complex eigenvalues with positive and negative real parts corresponding to the unstable and stable manifold directions, respectively. The first panel of figure 8(A) shows locations of identified saddle foci depicted in a 3-dimensional projection involving u_{11}, u_{31} and u_{41}. Another saddle focus was located along the segmented axis line beyond the depicted region. The state-space trajectories shown in the first panel of figure 8(A) belong to a high-complexity interictal attracting set with fractal dimension. The intersection of stable and unstable manifolds in the state space, whether due to homoclinic or heteroclinic tangencies, leads to the birth and extinction of high-complexity and/or chaotic dynamics (Grebogi *et al* 1983, 1986). The effect of network coupling is to therefore introduce saddle-type structures into the state space, which gives rise to emergent complexity in the dynamics. Local stability analysis of saddle equilibria over a range of β uncovered trends in the eigenvalues of the most unstable and stable manifolds found in the set (ξ_u and ξ_s), as estimated from the numerically computed Jacobian at those points (figure 8(B)). In the direction of decreasing β, the magnitudes of $\mathrm{Re}\,\xi_u > 0$ and $\mathrm{Re}\,\xi_s < 0$ became smaller, but the rate of decrease of $|\mathrm{Re}\,\xi_s|$ outpaced that of $\mathrm{Re}\,\xi_u$, so that the ratio of $\mathrm{Re}\,\xi_u$ to $|\mathrm{Re}\,\xi_s|$ increased. The overall change in $|\mathrm{Re}\,\xi_s|$ was larger as well, suggestive of a progressive erosion of stability with decreasing β over the given range.

As evidenced in figure 8(C), within the parameter ranges of β necessary for producing intermittent ictal- and interictal-like dynamics, the original periodic orbits have been replaced by a large-scale attractor consisting of a union of invariant sets and their basins—the ensemble relics of periodic orbits and small chaotic attractors that have become unstable or were created through successive bifurcations and attractor crises (Schaffer *et al* 1993, Szabo *et al* 1996). Although unstable, structures of saddle type can be visited intermittently along their stable manifold, and subsequently repelled in the direction of their unstable manifold to other regions of the state space. As such, the trajectory may transiently wander in the vicinity of a lower complexity saddle, exhibiting periodicities associated with the saddle structure. These periodicities show up in the orbit diagram of figure 8(C) as darker bands embedded within the larger high-complexity attractor, such as S1 and S2 corresponding to ictal bands. For sufficiently large β, the attractor periodicities are diffuse and spread out (indicating higher complexity dynamics) and the ictal regions are no longer visited, so that the dynamics are fully interictal. Sampling network dynamics from CRG 1, the mode response amplitude (u_{13}) at $\beta = 15$ displays small-amplitude fluctuations that are complex and irregular in appearance. At $\beta = 2$, however, large, cyclical deviations in the magnitude of u_{13} coincide with the occurrence of spontaneous SLEs. These exaggerated fluctuations in mode

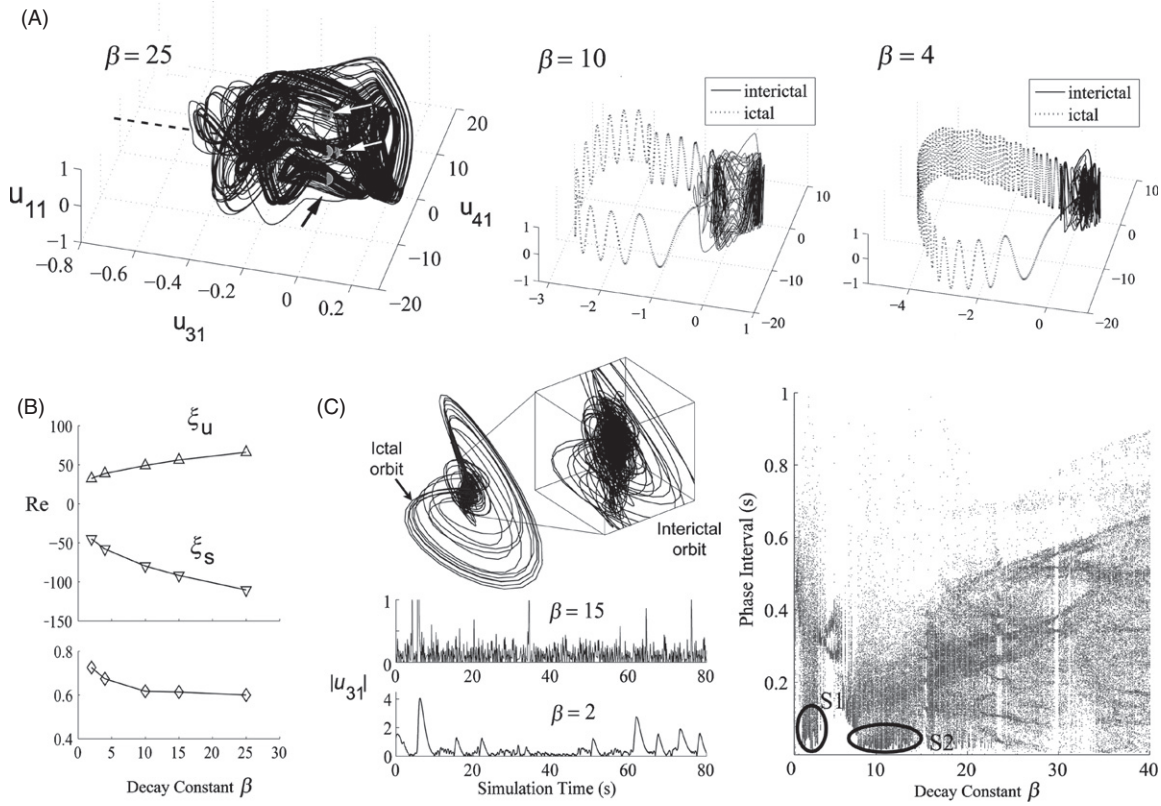

Figure 8. Mechanics of spontaneous seizure-like transitions. (A) At sufficiently high β, network dynamics remain bounded near the high-complexity interictal attracting set (arrows point to locations of saddle foci). At lower β, the trajectory can intermittently escape the high-complexity region and approach the periodic-like ictal saddle. (B) Real part of the eigenvalues of the most unstable (u) and stable (s) manifolds over a range of β. Below is the ratio $\mathrm{Re}\,\xi_U/|\mathrm{Re}\,\xi_S|$. (C) The magnitude of the mode response of CRG 1, u_{31}, reveals large cyclical deviations under epileptogenic conditions corresponding to seizure-like events, whereby the state of the system transitions from an interictal orbit to an ictal one. The transition is marked by a shift from a broader range of periodicities to a narrower, more regular band at a higher frequency (S1 or S2).

response, associated with sufficiently low values of β, are the result of feedback destabilization brought about by the enhanced integrating functionality of modes with increased duration and area. The larger magnitude deviations correspond to the state trajectory escaping the interictal region more readily and approaching the ictal region for a longer duration, thereby producing lengthier, more pronounced SLEs. This is illustrated in figure 8(A), whereby the number of periods within an ictal burst increases with decreasing β, but the frequency of the discharges remains almost the same (S1 and S2 in the orbit diagram share similar phase interval for different values of β). Disruption of negative feedback regulation at low β has the greatest effect on network activity; when negative feedback coupling is severed altogether, the network operates in a continuous epileptiform mode of tonic spiking or bursting (i.e. *status epilepticus*), as seen in figure 7(A). Negative feedback helps to maintain the complexity of network activity and balance excitability, but with destabilization of the network occurring at low ranges of β, the network transiently enters a pathological mode of operation, signaling a breakdown in the feedback regulation of 'normal' network activity. The dynamics of the network essentially become bimodal, alternating intermittently between the interictal and ictal orbits.

4. Discussion

Through application of signal processing and nonlinear system identification techniques to real data recorded from the isolated intact hippocampus in the low-Mg^{2+}/high-K^+ model of epilepsy, we established a positive correlation between changes in spectral energy content of hippocampal CA3 pyramidal cell responses to Gaussian white noise stimulation and changes in first-order kernel size and duration. More succinctly, an increase in neuronal excitability corresponded to increased kernel duration, whereas decreased excitability was associated with decreased kernel duration. Subsequently, using the CRG mathematical network model of coupled nonlinear oscillators, we demonstrated that changes in first-order kernel duration can be related to underlying specific changes of the model's parameters. By varying the β parameter, and hence varying the decay length of the exponential integrating mode (which is analogous in function to the first-order kernel), we induced quantitative changes in the CRG model's network dynamics, and were able to generate spontaneous SLEs that were similar in appearance and dynamics to those generated in the low-Mg^{2+}/high-K^+ model of epilepsy, thus indicating that a pathological change in network excitability had occurred as a result of modifying β.

Since the kernels encode the input–output dynamics of the system, it is expected that any fundamental modification of the

system affecting its dynamic response to external stimulation, or to synaptic inputs from other neurons in a network, for example, would be reflected by changes in the measured kernels. Increased kernel duration is one characteristic of the kernels that is apparent under hyperexcitable conditions. Intuitively, this makes sense, because a longer kernel duration reflects greater integration capacity, which results in increased rates of energy accumulation in the network. The physiological correlate of this is typically an enlargement or elongation of the post-synaptic response (for example, see Poolos and Kocsis 1990). The large, cyclical swings in excitation level observed for low values of β are a manifestation of abnormal network feedback regulation of excitability (see figure 8): the mechanisms of energy accumulation and dissipation have become unbalanced, transiently destabilizing the system and leading to over- and under-compensation of network activity, as evidenced by the dynamics of mode response variable u_{3n} (figure 8(C)). The large-amplitude fluctuations in u_{3n} correspond to seizure-like episodes that see the state trajectory momentarily leave the high-complexity interictal region and enter an ictal orbit, as illustrated in the state space projections of u_{11}, u_{31} and u_{41} in figure 8(A). The seizure-like episodes are interspersed by quieter periods of more-or-less balanced activity, as is consistent with the acute-onset model of epilepsy, with the system able to sustain recurring transitions between ictal and interictal states, in effect becoming a 'seizure engine'.

The spontaneous seizure-like transitions exhibited in the mathematical hippocampal network model differ categorically from transitions that are induced by parameter changes or by the presence of noise fluctuations in the model (figure 7(B)). Classically, parameter drifts cause transitions by way of bifurcations or changes in the stability of fixed points or orbits in state space. Transitions produced by noise fluctuations can occur in a similar manner; often, the process involves a hysteresis loop that gives rise to bistability. This is how paroxysmal transitions are explained in a bistable lumped-parameter model of absence epilepsy, wherein it is hypothesized that random fluctuations introduced into the system by noise in cortical and sensory inputs are necessary for epileptiform transitions to be able to occur (Suffczynski *et al* 2004); without noise fluctuations, transitions do not take place (Suffczynski *et al* 2005). The CRG network model, however, is a model exhibiting intermittency and recurrence in the absence of additive stimulation or noise fluctuations. Under simulated epileptogenic conditions, transitions occur unprovoked between the interictal and ictal regions of a chaotic attractor (figure 8(C)), with the trajectory visiting the neighborhood of each region intermittently. One mechanism that helps to facilitate occurrence of SLE transitions in the model (but is not required for them to occur) is associated with large magnitudes of negative feedback coupling; that is, when sizable swings in excitation level (i.e. magnitude of the mode response amplitude, u_{3n}) are prevalent: at SLE onset, the negative coupling can switch and become excitatory in nature, when the value of the modulatory function $S_{\phi,n}$ of CRG 1 or CRG 2 becomes lower than -1 in the course of the dynamic evolution of the system. A net inhibitory effect occurs in the region $-1 \leqslant S_{\phi,n} < 0$, with the phase advance of the limit cycle slowing and eventually sticking at $S_{\phi,n} = -1$. Below -1, the effect becomes excitatory again. This facilitating switch from inhibition to partial excitation under epileptiform network conditions is in agreement with experimental reports of the transient excitatory influence of GABAergic mechanisms in promoting seizure-like activity (Derchansky *et al* 2008, Fujiwara-Tsukamoto *et al* 2006, Marty and Llano 2005).

The results of the CRG model allude to a plausible contributing mechanism for the emergence of spontaneous, recurrent SLEs in the hippocampal system under low-Mg^{2+}/high-K^+ conditions: the SLEs generated by the model are fairly consistent in duration, lasting between 2 and 8 s of simulated time (the peak duration depends on parameterization); the time scales of biological SLEs, however, have been observed to vary in duration from tens of milliseconds to minutes in length (Borck and Jefferys 1999, Derchansky *et al* 2004). To produce such long-lasting SLEs in the model as the latter would require enlargement of the integrating mode such that its decay profile approaches the same order of length in time. Already, the size of the integrating mode needed to produce SLEs in the model is significantly larger than the size of the first-order kernels measured experimentally, although the relative change in kernel size going from normal to epileptogenic conditions is roughly comparable. One explanation is network size: a larger network can sustain longer lasting SLEs than a smaller network; this is evident when comparing the duration of long-lasting or contiguous ictal-like events in hippocampal slices (tens of seconds) to those in the intact hippocampus (several minutes). But the result is also suggestive of a dynamic process with a time constant much larger than any ion-channel kinetics or membrane capacitances can adequately account for.

One dynamic process consistent with the extended time scale of SLEs—as well as being innately involved in mediating network excitability—is the regulation of extracellular potassium concentration, $[K^+]_e$. When mechanisms that regulate $[K^+]_e$ are disrupted, or if $[K^+]_e$ is artificially elevated (as is done in many experimental models of epilepsy), seizure-like activities can arise spontaneously (Rutecki *et al* 1985). Pathological regulation of $[K^+]_e$ manifests as phasic over- and under-shoots in concentration level; these cyclic deviations from the baseline concentration coincide with the occurrence of SLEs, and have the same time course as SLEs (Dreier and Heinemann 1991). Similarities exist with the mode response amplitude, u_{3n}, in the CRG model. Therefore, u_{3n} may have a physical interpretation in being the variable that relates to the time evolution of the extracellular potassium concentration.

While $[K^+]_e$ has many effects, including affecting chloride reversal potential, and can act independently of synapses to non-selectively depolarize the network and coordinate synchronous activity (Park and Durand 2006, Yaari *et al* 1986), $[K^+]_e$ also exerts a modulatory influence on certain varieties of synaptic receptors; for example, elevated $[K^+]_e$ enhances excitatory NMDA receptor activation (Poolos and Kocsis 1990). Although persistently high $[K^+]_e$ has a depressant effect on neuronal activity, phasic extracellular

potassium accumulation is hypothesized to form part of a positive feedback loop involving $[K^+]_e$ and neuronal activation (Bazhenov *et al* 2008, Traynelis and Dingledine 1988), one that likely contributes to initiation of spontaneous, recurrent SLEs. Namely, as $[K^+]_e$ is elevated, it depolarizes cell membranes, modulates synaptic activity and increases neuronal firing and recruitment in the network (Frohlich *et al* 2008); this in turn leads to higher $[K^+]_e$, as the intensifying neuronal discharges expel more potassium into the local extracellular environment. At some point, negative feedback mechanisms such as GABAergic inhibition and astrocytic uptake of excess extracellular potassium (Walz 2000) compensate to bring $[K^+]_e$ back down, setting the system up for a new cycle. The CRG hippocampal network model already includes negative feedback in a form that emulates inhibitory neuronal connectivity, but it does not take into account the effect of glial cells or their interactions, which would necessitate development of a system-level representation of glial cell dynamics amenable to implementation in one or more CRG units. There has been recent interest in the role of glial cell dysfunction in epileptogenesis as related to impaired extracellular potassium regulation by astrocytes (Binder and Steinhauser 2006, Djukic *et al* 2007).

The CRG model is limited by its coarse level of resolution when accounting for detailed structures or mechanisms at the cellular level. The model readily elucidates system-level properties and mechanisms, such as the role of opposing feedback in regulating network activity, but other approaches such as conductance-based models would be more useful for investigating specific receptor or channel-related properties. A second limitation is that the current hippocampal network model does not incorporate specific mechanisms for dealing with short or long-term plasticity. Bifurcations in network dynamics are induced by manually changing parameter values or coupling strengths, whereas activity-dependent plasticity would bring about such changes in a dynamic manner. For example, a comparison of the model and biological data in figures 5 and 6 reveals similarities in dynamics, but the biological data show more diversity in the dynamics over time, with greater variation of waveforms and bursting. In other words, the dynamics are more nonstationary. This is perceptible in figures 6(A) and (B), as the maximum Lyapunov exponent during the ictal episode fluctuates when estimated from the biological trace but remains more constant when estimated from the model trace. In the biological data, it may be possible to distinguish different states associated with the SLE, such as a pre- and post-ictal period, characterized by distinct dynamics and transitions (Chiu *et al* 2006, Iasemidis 2003, 2003a, 2003b, 2004), whereas in the model there are really only two principal dynamic states—ictal and interictal (even though in the case of mixed interictal-like dynamics, the network does shift intermittently between different types of activity having distinct patterning or rhythmicity). Incorporating forms of plasticity into the model would be expected to increase non-stationarity and complexity in the model, thus narrowing the phenomenological gap between the model and the physiological system.

Acknowledgments

This work was supported by grants from the Natural Sciences and Engineering Research Council of Canada and from the Canadian Institutes of Health Research.

References

Bardakjian B L and Diamant N E 1994 A mapped clock oscillator model for transmembrane electrical rhythmic activity in excitable cells *J. Theor. Biol.* **166** 225–35

Bazhenov M, Timofeev I, Frohlich F and Sejnowski T J 2008 Cellular and network mechanisms of electrographic seizures *Drug Discov. Today Dis. Models* **5** 45–57

Behrens C J, Van Den Boom L P and Heinemann U 2007 Effects of the GABA(A) receptor antagonists bicuculline and gabazine on stimulus-induced sharp wave-ripple complexes in adult rat hippocampus *in vitro Eur. J. Neurosci.* **25** 2170–81

Bergey G K and Franaszczuk P J 2001 Epileptic seizures are characterized by changing signal complexity *Clin. Neurophysiol.* **112** 241–9

Binder D K and Steinhauser C 2006 Functional changes in astroglial cells in epilepsy *Glia* **54** 358–68

Borck C and Jefferys J G 1999 Seizure-like events in disinhibited ventral slices of adult rat hippocampus *J. Neurophysiol.* **82** 2130–42

Buzsaki G 2002 Theta oscillations in the hippocampus *Neuron* **33** 325–40

Buzsaki G and Draguhn A 2004 Neuronal oscillations in cortical networks *Science* **304** 1926–9

Carvalho T P and Buonomano D V 2009 Differential effects of excitatory and inhibitory plasticity on synaptically driven neuronal input–output functions *Neuron* **61** 774–85

Chakravarthy N, Tsakalis K, Sabesan S and Iasemidis L 2009 Homeostasis of brain dynamics in epilepsy: a feedback control systems perspective of seizures *Ann. Biomed. Eng.* **37** 565–85

Chiu A W, Jahromi S S, Khosravani H, Carlen P L and Bardakjian B L 2006 The effects of high-frequency oscillations in hippocampal electrical activities on the classification of epileptiform events using artificial neural networks *J. Neural Eng.* **3** 9–20

Derchansky M, Jahromi S S, Mamani M, Shin D S, Sik A and Carlen P L 2008 Transition to seizures in the isolated immature mouse hippocampus: a switch from dominant phasic inhibition to dominant phasic excitation *J. Physiol.* **586** 477–94

Derchansky M, Rokni D, Rick J T, Wennberg R, Bardakjian B L, Zhang L, Yarom Y and Carlen P L 2006 Bidirectional multisite seizure propagation in the intact isolated hippocampus: the multifocality of the seizure 'focus' *Neurobiol. Dis.* **23** 312–28

Derchansky M, Shahar E, Wennberg R A, Samoilova M, Jahromi S S, Abdelmalik P A, Zhang L and Carlen P L 2004 Model of frequent, recurrent, and spontaneous seizures in the intact mouse hippocampus *Hippocampus* **14** 935–47

Djukic B, Casper K B, Philpot B D, Chin L S and McCarthy K D 2007 Conditional knock-out of Kir4.1 leads to glial membrane depolarization, inhibition of potassium and glutamate uptake, and enhanced short-term synaptic potentiation *J. Neurosci.* **27** 11354–65

Dreier J P and Heinemann U 1991 Regional and time dependent variations of low Mg2+ induced epileptiform activity in rat temporal cortex slices *Exp. Brain Res.* **87** 581–96

Dudek F E and Staley K J 2007 How does the balance of excitation and inhibition shift during epileptogenesis? *Epilepsy Curr.* **7** 86–8

Frohlich F, Bazhenov M, Iragui-Madoz V and Sejnowski T J 2008 Potassium dynamics in the epileptic cortex: new insights on an old topic *Neuroscientist* **14** 422–33

Fujiwara-Tsukamoto Y, Isomura Y and Takada M 2006 Comparable GABAergic mechanisms of hippocampal seizurelike activity in posttetanic and low-Mg2+ conditions *J. Neurophysiol.* **95** 2013–19

Gaiarsa J L, Caillard O and Ben-Ari Y 2002 Long-term plasticity at GABAergic and glycinergic synapses: mechanisms and functional significance *Trends Neurosci.* **25** 564–70

Goutagny R, Jackson J and Williams S 2009 Self-generated theta oscillations in the hippocampus *Nat. Neurosci.* **12** 1491–3

Grebogi C, Ott E and Yorke J A 1983 Crises, sudden changes in chaotic attractors, and transient chaos *Phys. D: Nonlinear Phenom.* **7** 181–200

Grebogi C, Ott E and Yorke J A 1986 Critical exponent of chaotic transients in nonlinear dynamical systems *Phys. Rev. Lett.* **57** 1284–7

Hasselmo M E, Schnell E and Barkai E 1995 Dynamics of learning and recall at excitatory recurrent synapses and cholinergic modulation in rat hippocampal region CA3 *J. Neurosci.* **15** 5249–62

Hooke R and Jeeves T A 1961 'Direct search' solution of numerical and statistical problems *JACM* **8** 212–29

Iasemidis L D 2003 Epileptic seizure prediction and control *IEEE Trans. Biomed. Eng.* **50** 549–58

Iasemidis L D, Pardalos P M, Shiau D S, Chaovalitwongse W, Narayanan K, Kumar S, Carney P R and Sackellares J C 2003a Prediction of human epileptic seizures based on optimization and phase changes of brain electrical activity *Optim. Meth. Softw.* **18** 81–104

Iasemidis L D, Principe J C and Sackellares J C 2000 Measurement and quantification of spatiotemporal dynamics of human epileptic seizures *Nonlinear Biomedical Signal Processing* ed M Akay (Piscataway, NJ: IEEE Press) pp 294–318

Iasemidis L D, Shiau D S, Chaovalitwongse W, Sackellares J C, Pardalos P M, Principe J C, Carney P R, Prasad A, Veeramani B and Tsakalis K 2003b Adaptive epileptic seizure prediction system *IEEE Trans. Biomed. Eng.* **50** 616–27

Iasemidis L D, Shiau D S, Sackellares J C, Pardalos P M and Prasad A 2004 Dynamical resetting of the human brain at epileptic seizures: application of nonlinear dynamics and global optimization techniques *IEEE Trans. Biomed. Eng.* **51** 493–506

Kang E E, Zalay O C, Cotic M, Carlen P L and Bardakjian B L 2010 Transformation of neuronal modes associated with low-Mg^{2+}/high-K^{+} conditions in an *in vitro* model of epilepsy *J. Biol. Phys.* **36** 95–107

Khalilov I, Esclapez M, Medina I, Aggoun D, Lamsa K, Leinekugel X, Khazipov R and Ben-Ari Y 1997 A novel *in vitro* preparation: the intact hippocampal formation *Neuron* **19** 743–9

Kim U, Sanchez-Vives M V and McCormick D A 1997 Functional dynamics of GABAergic inhibition in the thalamus *Science* **278** 130–4

Kubota D, Colgin L L, Casale M, Brucher F A and Lynch G 2003 Endogenous waves in hippocampal slices *J. Neurophysiol.* **89** 81–9

Marder E and Thirumalai V 2002 Cellular, synaptic and network effects of neuromodulation *Neural. Netw.* **15** 479–93

Marmarelis V Z 1993 Identification of nonlinear biological systems using Laguerre expansions of kernels *Ann. Biomed. Eng.* **21** 573–89

Marple S L 1999 Computing the discrete-time 'analytic' signal via FFT *IEEE Trans. Signal Process.* **47** 2600–3

Marty A and Llano I 2005 Excitatory effects of GABA in established brain networks *Trends Neurosci.* **28** 284–9

Nair S P, Shiau D S, Principe J C, Iasemidis L D, Pardalos P M, Norman W M, Carney P R, Kelly K M and Sackellares J C 2009 An investigation of EEG dynamics in an animal model of temporal lobe epilepsy using the maximum Lyapunov exponent *Exp. Neurol.* **216** 115–21

Ogura H 1985 Estimation of Wiener kernels of a nonlinear system and a fast algorithm using digital laguerre filters *Proc. 15th NIBB Conf. (Okazaki, Japan)* pp 14–62

Ottman R, Annegers J F, Risch N, Hauser W A and Susser M 1996 Relations of genetic and environmental factors in the etiology of epilepsy *Ann. Neurol.* **39** 442–9

Palmini A, Andermann F, Olivier A, Tampieri D, Robitaille Y, Andermann E and Wright G 1991 Focal neuronal migration disorders and intractable partial epilepsy: a study of 30 patients *Ann. Neurol.* **30** 741–9

Park E H and Durand D M 2006 Role of potassium lateral diffusion in non-synaptic epilepsy: a computational study *J. Theor. Biol.* **238** 666–82

Poolos N P and Kocsis J D 1990 Elevated extracellular potassium concentration enhances synaptic activation of *N*-methyl-*D*-aspartate receptors in hippocampus *Brain Res.* **508** 7–12

Rutecki P A, Lebeda F J and Johnston D 1985 Epileptiform activity induced by changes in extracellular potassium in hippocampus *J. Neurophysiol.* **54** 1363–74

Schaffer W M, Kendall B E, Tidd C W and Olsen L F 1993 Transient periodicity and episodic predictability in biological dynamics *IMA J. Math. Appl. Med. Biol.* **10** 227–47

Scharfman H E 2007 The neurobiology of epilepsy *Curr. Neurol. Neurosci. Rep.* **7** 348–54

Strata F 1998 Intrinsic oscillations in CA3 hippocampal pyramids: physiological relevance to theta rhythm generation *Hippocampus* **8** 666–79

Suffczynski P, Kalitzin S and Lopes Da Silva F H 2004 Dynamics of non-convulsive epileptic phenomena modeled by a bistable neuronal network *Neuroscience* **126** 467–84

Suffczynski P, Lopes da Silva F, Parra J, Velis D and Kalitzin S 2005 Epileptic transitions: model predictions and experimental validation *J. Clin. Neurophysiol.* **22** 288–99

Sutula T, Cascino G, Cavazos J, Parada I and Ramirez L 1989 Mossy fiber synaptic reorganization in the epileptic human temporal lobe *Ann. Neurol.* **26** 321–30

Szabo K G, Lai Y C, Tel T and Grebogi C 1996 Critical exponent for gap filling at crisis *Phys. Rev. Lett.* **77** 3102–5

Traynelis S F and Dingledine R 1988 Potassium-induced spontaneous electrographic seizures in the rat hippocampal slice *J. Neurophysiol.* **59** 259–76

Trujillo L, Olague G, Legrand P and Lutton E 2007 Regularity based descriptor computed from local image oscillations *Opt. Exp.* **15** 6140–5

Varela J A, Sen K, Gibson J, Fost J, Abbott L F and Nelson S B 1997 A quantitative description of short-term plasticity at excitatory synapses in layer 2/3 of rat primary visual cortex *J. Neurosci.* **17** 7926–40

Walz W 2000 Role of astrocytes in the clearance of excess extracellular potassium *Neurochem. Int.* **36** 291–300

Wilson M and Bower J M 1992 Cortical oscillations and temporal interactions in a computer simulation of piriform cortex *J. Neurophysiol.* **67** 981–95

Wu C, Shen H, Luk W P and Zhang L 2002 A fundamental oscillatory state of isolated rodent hippocampus *J. Physiol.* **540** 509–27

Yaari Y, Konnerth A and Heinemann U 1986 Nonsynaptic epileptogenesis in the mammalian hippocampus *in vitro*: II. Role of extracellular potassium *J. Neurophysiol.* **56** 424–38

Zalay O C and Bardakjian B L 2008 Mapped clock oscillators as ring devices and their application to neuronal electrical rhythms *IEEE Trans. Neural Syst. Rehabil. Eng.* **16** 233–44

Zalay O C and Bardakjian B L 2009 Theta phase precession and phase selectivity: a cognitive device description of neural coding *J. Neural Eng.* **6** 036002